



## Facile self-assembly synthesis of $\gamma$ -Fe<sub>2</sub>O<sub>3</sub> /graphene oxide for enhanced photo-Fenton reaction

Feifei Wang<sup>a, b, d</sup>, Xiaolin Yu<sup>d</sup>, Maofa Ge<sup>d</sup>, Sujun Wu<sup>a, b, \*</sup>, Juan Guan<sup>a, b</sup>, Junwang Tang<sup>c</sup>, Xiao Wu<sup>d</sup>, Robert O. Ritchie<sup>b, e</sup>

<sup>a</sup> School of Materials Science and Engineering, Beihang University, Beijing, 100191, China

<sup>b</sup> Intl. Research Centre for Advanced Structural and Bio-Materials, Beihang University, Beijing, 100191, China

<sup>c</sup> Solar Energy & Advanced Materials Research Group, Department of Chemical Engineering, University College London, London, WC1E 7JE, UK

<sup>d</sup> Institute of Chemistry, Chinese Academy of Sciences, Beijing, 100190, China

<sup>e</sup> Department of Materials Science & Engineering, University of California, Berkeley, CA, 94720, USA

### ARTICLE INFO

#### Article history:

Received 13 November 2018

Received in revised form

28 December 2018

Accepted 7 January 2019

Available online 29 January 2019

#### Keywords:

Photocatalysis

Fenton-like reaction

Self-assembly

Graphene oxide

Methylene blue degradation

### ABSTRACT

A novel self-assembly method was developed to prepare a  $\gamma$ -Fe<sub>2</sub>O<sub>3</sub>/graphene oxide (GO) heterogeneous catalyst that showed excellent synergy between photocatalysis and Fenton-like reactions. The  $\gamma$ -Fe<sub>2</sub>O<sub>3</sub>/GO catalyst prepared on the iron plates demonstrated efficient and reproducible catalytic activities for water treatment. It takes only 80 min to degrade 50 mg L<sup>-1</sup> methylene (MB) completely, which is the main non-biodegradable dye in wastewater from the textile industry. The heterogeneous catalyst is stable over a wide range of pH (from 2.0 to 10.2) for MB degradation, and can be easily extracted from solution and repeatedly used with little loss of catalytic activity. The high activity and stability of the catalyst system can be attributed to charge separation between  $\gamma$ -Fe<sub>2</sub>O<sub>3</sub> and GO, which could accelerate Fenton-like process and photocatalysis. In addition, the dominant reactive oxidant species responsible for the MB degradation, including the hydroxyl radicals ( $\bullet$ OH) and holes (h<sup>+</sup>), were trapped on the surface of the  $\gamma$ -Fe<sub>2</sub>O<sub>3</sub>/GO composite, as proved by a free-radical quenching experiment. The  $\gamma$ -Fe<sub>2</sub>O<sub>3</sub>/GO heterogeneous catalyst could potentially provide a solution for removal of non-biodegradable dyes from wastewater in the textile industry.

© 2019 Elsevier Ltd. All rights reserved.

### 1. Introduction

One of the adverse consequences of the modern industrialization is severe environmental pollution. It is extremely necessary to seek efficient and more importantly green technologies to remove these pollutants. One prevalent pollutant is the colorful dye from various industries such as textiles, printing, food, paper, leather and cosmetics; this has become a serious environmental problem due to its high toxicity and slow self-degradation under natural conditions (Munoz et al., 2015; Techalertmanee et al., 2015). There is therefore an increasing imperative to develop facile and efficient processes to eliminate these dye pollutants, from the vital perspective of benefitting the environment and human health (Zhang et al., 2018b).

Methods such as adsorption and flocculation have been used to remove dye pollutants from wastewater (Dong et al., 2015; Zhang et al., 2015) although many such treatment methods do not clean the pollutants completely and can produce secondary waste products which require further processing (Muthukrishnaraj et al., 2015). Of note though is that chemical oxidation, or the conventional Fenton process, is one of the most efficient, low cost and convenient advanced oxidation processes (AOPs) for wastewater treatment (Jin et al., 2018), although strict reaction conditions, such as highly acidic conditions (pH < 4), and the generation of substantial iron sludge and waste catalyst remain a challenge (Triki et al., 2014).

Recently, an iron-based solid catalyst termed heterogeneous Fenton oxidative has offered a promising alternative. Iron and iron oxides have been widely used as heterogeneous Fenton catalysts because of their inexpensive, safe and environmental friendly properties (Wang et al., 2008). However, they often suffer from some critical drawbacks for the industrial application, such as low utilization efficiency of H<sub>2</sub>O<sub>2</sub>, the narrow working pH range and

\* Corresponding author. School of Materials Science and Engineering, Beihang University, Beijing, 100191, China.

E-mail address: [wusj@buaa.edu.cn](mailto:wusj@buaa.edu.cn) (S. Wu).

easy deactivation due to the generation of  $\text{Fe}(\text{OH})_3$  (Qiu et al., 2015).

To improve the catalytic activity and stability of these iron-based heterogeneous Fenton catalysts, various supports such as Nafion, resin, zeolite, clays and carbon, have been studied (Cheng et al., 2004; Guo et al., 2014; Liu et al., 2016; Macedo et al., 2016; Parra et al., 2004). In this regard, graphene oxide (GO) has attracted considerable attention as one of the most promising supports because of its large surface area. Furthermore, GO provides high accessibility of reactants towards its active sites to diminish limitations in mass transfer during catalysis (Zhang et al., 2018b); further, the oxygenated functional groups may act to immobilize iron oxide (Chen and Chen, 2018; Liu et al., 2018). Up to now, progress has been made in preparing GO supported iron heterogeneous Fenton catalysts via various pathways, including hydrothermal methods, co-precipitation techniques, sol-gel methods (Dong et al., 2018; Guo et al., 2013; Yu et al., 2016; Zhou et al., 2018). However, these method usually draws some inevitable shortcomings, such as long reaction time, high reaction temperature and the use of toxic solvent. Han et al. reported the one-step synthesis of  $\alpha\text{-Fe}_2\text{O}_3$ /graphene composites by hydrothermal treatment at 180 °C for 24 h (Han et al., 2014). Qiu et al. fabricated the  $\text{Fe}_2\text{O}_3$ /graphene aerogel by a Stober-like method at high temperature and high pressure using toxic acetonitrile as a co-solvent (Qiu et al., 2015). Moreover, the complexity and protracted nature of these techniques severely limit their efficiency and scalability in synthesizing target products (Zhang et al., 2017). It is urgent to develop a facile and efficient method for the preparation of the graphene supported iron heterogeneous catalyst.

Accordingly, we reasoned that there was significant utility to explore a facile way of preparing heterogeneous catalysts specifically from the perspective of improving efficiency and saving time. Consequently, in this study, a magnetically separable  $\gamma\text{-Fe}_2\text{O}_3$ /GO composite was synthesized using a simple self-assembly method for a short time at low temperature. Compared to existing techniques (Li et al., 2017; Maleki, 2016), this self-assembly method exhibits excellent scalability, facile tunability and high efficiency. The as-prepared product need not undergo the separation process of filtration or centrifugation, which can be readily peeled from the iron plate after drying. The efficiency of the  $\gamma\text{-Fe}_2\text{O}_3$ /GO composite for the MB degradation is studied and the related photo-Fenton degradation and mineralization mechanisms are discussed.

## 2. Experimental

### 2.1. Reagents and materials

Graphite powder (99.998 wt.%, 200 mesh) was purchased from Alfa Aesar Ltd. (Shanghai, China). The  $\gamma\text{-Fe}_2\text{O}_3$  nanoparticles were purchased from Aladdin (Shanghai, China), and its size is about 10 nm–30 nm (shown in Fig. S1). Potassium permanganate ( $\text{KMnO}_4$ , 99.5 wt.%), hydrogen peroxide ( $\text{H}_2\text{O}_2$ , 30 wt.%), methanol ( $\text{CH}_3\text{OH}$ , 99.9 wt.%) and sulfuric acid ( $\text{H}_2\text{SO}_4$ , 98 wt.%) were all obtained from Beijing Chemical Works (Beijing, China). Pure iron plate (99.9 wt.%) plates (10 × 10 × 5 mm), were purchased from Anyang Iron & Steel Group Co Ltd. The methylene blue (MB, 99.5 wt.%) with a molecular formula  $\text{C}_{16}\text{H}_{18}\text{ClN}_3\text{S} \cdot 3\text{H}_2\text{O}$ , p-Benzoquinone (BQ, 99 wt.%) triethanolamine (TEOA) and terephthalic acid (TA, 99 wt.%) used in this study were obtained from Aladdin Chemical Ltd (Shanghai, China). All chemicals were of analytical grade and used without further purification. Deionized (DI) water was utilized throughout the synthesis process.

### 2.2. Fabrication of the $\gamma\text{-Fe}_2\text{O}_3$ /GO composite

Graphene oxide (GO) was prepared from graphite powder using a modified Hummers method and the  $\gamma\text{-Fe}_2\text{O}_3$ /GO composite was obtained by self-assembly method (Cao et al., 2013; William and Offeman, 1958). The synthetic procedure for the  $\gamma\text{-Fe}_2\text{O}_3$ /GO composite is illustrated in Scheme 1. First, iron plates substrate was mechanically polished by a series of silicon carbide papers followed by polishing with alumina compounds. Once their surface roughness became less than  $\sim 1 \mu\text{m}$ , the plates were ultrasonically cleaned in acetone, alcohol and deionized water in sequence for 15 min second, the iron plates were then immersed in the GO solution at 40 °C where the  $\gamma\text{-Fe}_2\text{O}_3$ /GO films were gradually formed on the surface of the iron. After 2 h, the iron plates together with the  $\gamma\text{-Fe}_2\text{O}_3$ /GO films were taken out of the solution and then oven dried at 60 °C for a further 2 h. Following such processing, the  $\gamma\text{-Fe}_2\text{O}_3$ /GO films could be readily peeled from the iron substrate before being cut into small pieces for catalytic evaluation.

### 2.3. Characterization

The physicochemical characteristics of GO and  $\gamma\text{-Fe}_2\text{O}_3$ /GO composite were characterized by different techniques. The detail information was given in supporting information (SI).

### 2.4. Test of catalytic activity

The photocatalytic activities of the as-prepared catalyst were evaluated by photocatalytic degradation in MB aqueous solution. A 250 W high pressure Hg lamp was located 15 cm above the center of the solution as the UV irradiation source. 10 mg of catalysts was added to the 50 ml MB solution ( $50 \text{ mg L}^{-1}$ ). Prior to irradiation, the catalytic systems without  $\text{H}_2\text{O}_2$  were stirred in the dark for 30 min to establish adsorption-desorption equilibrium (shown in Fig. S2). Subsequently, the heterogeneous Fenton-like reaction was started when the lamp was turned on and 2.5 ml of  $\text{H}_2\text{O}_2$  was added. About 2 ml solution was withdrawn at given time intervals and the catalysts collected by magnetic separation. The UV–vis absorbance of the MB solution was measured on UV–vis spectroscopy at 664 nm.

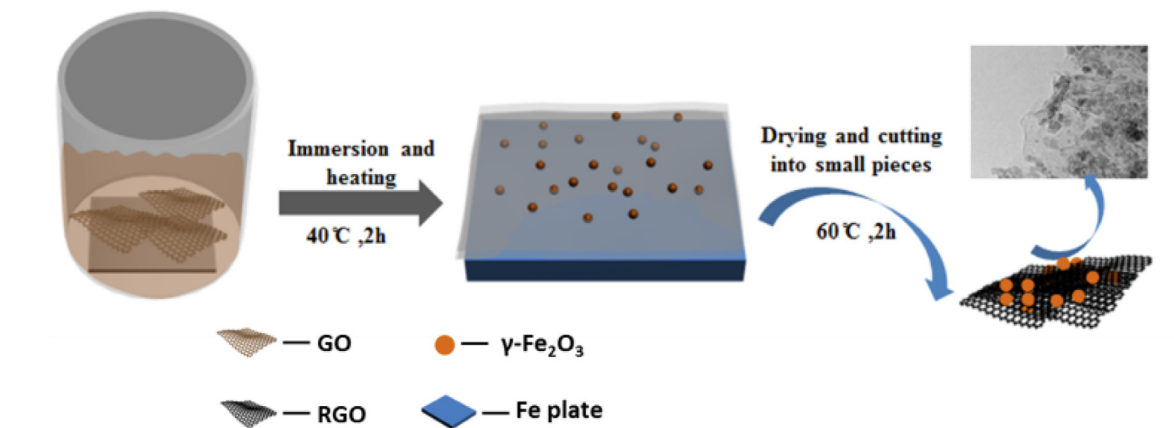
### 2.5. Measurement of radical formation

In the  $\gamma\text{-Fe}_2\text{O}_3$ /GO +  $\text{H}_2\text{O}_2$ +UV system, hydroxyl radicals ( $\bullet\text{OH}$ ), superoxide anion radicals ( $\bullet\text{O}_2^-$ ) and holes ( $\text{h}^+$ ) were detected the quenching experiment, the generation of  $\bullet\text{OH}$  was detected by using photoluminescence spectra (PL spectra). The detail information was given in supporting information (SI).

## 3. Results and discussion

### 3.1. Composition and structure characterizations

The XRD patterns in Fig. 1a represent typical crystalline structures of the graphite, GO and  $\gamma\text{-Fe}_2\text{O}_3$ /GO composite. The strong peak at  $2\theta = 26.9^\circ$  in the graphite curve disappeared when the graphite was oxidized to become GO. Instead, a strong peak at  $2\theta = 10.6^\circ$  appeared (shown in GO of Fig. 1a) which confirmed that the graphite had successfully converted to GO with a larger layer spacing of 0.8 nm (Li et al., 2013). The thickness of the GO was also examined using AFM and found to be approximately 1.4 nm (as shown in Fig. S3 in the Supplementary Information). The peaks in the XRD patterns of as-prepared  $\gamma\text{-Fe}_2\text{O}_3$ /GO composite at  $2\theta = 30.5^\circ$ ,  $35.8^\circ$ ,  $43.5^\circ$ ,  $53.8^\circ$ ,  $57.4^\circ$  and  $63.0^\circ$  are respectively indexed as the (220), (311), (400), (422), (511) and (440) crystal planes of  $\gamma\text{-Fe}_2\text{O}_3$  (JCPDS 25–1402).



Scheme 1. Illustrative procedure for synthesis of the  $\gamma$ -Fe<sub>2</sub>O<sub>3</sub>/GO composite.

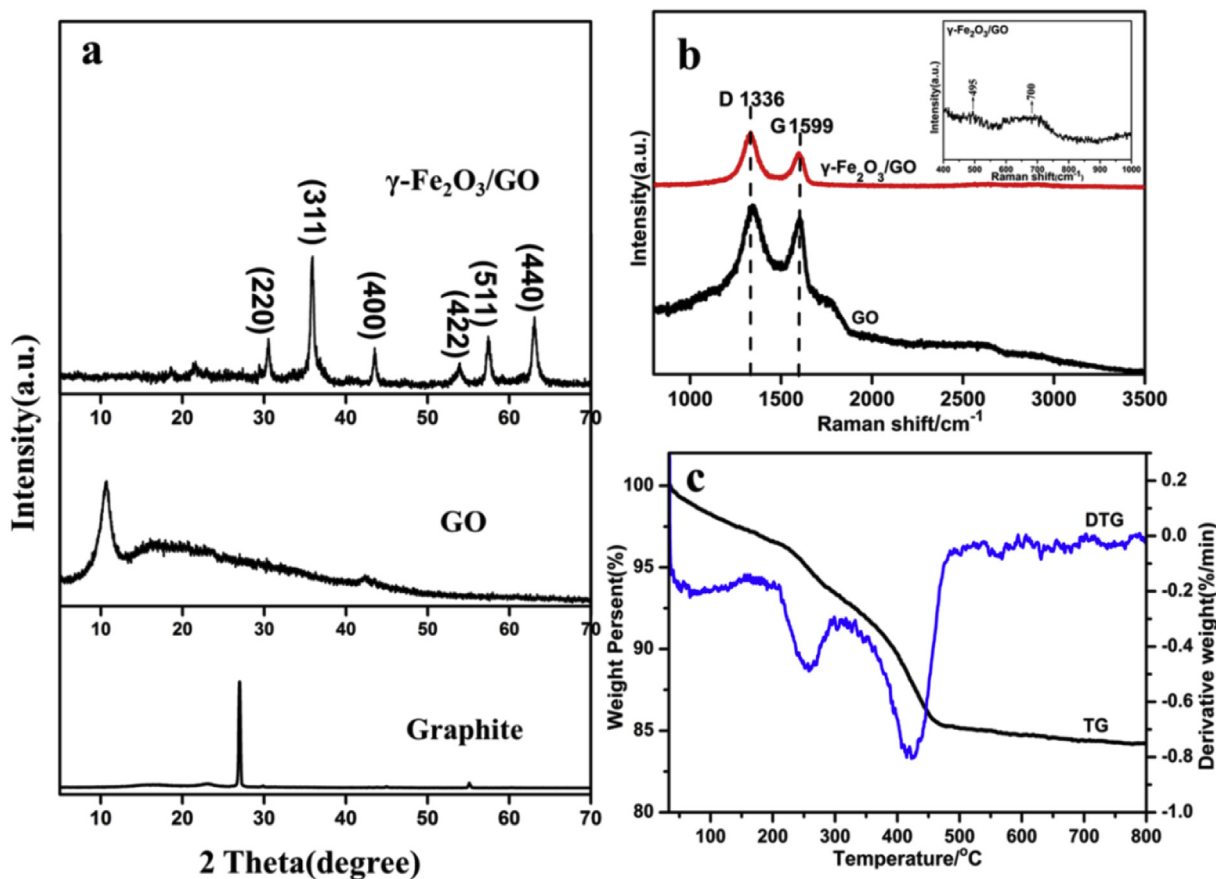


Fig. 1. (a) XRD patterns of graphite, GO and  $\gamma$ -Fe<sub>2</sub>O<sub>3</sub>/GO composite, (b) Raman spectra of GO and the  $\gamma$ -Fe<sub>2</sub>O<sub>3</sub>/GO composites, (c) TG and DTG curves of the  $\gamma$ -Fe<sub>2</sub>O<sub>3</sub>/GO composite.

Raman spectroscopy was used to verify the co-existence of  $\gamma$ -Fe<sub>2</sub>O<sub>3</sub> and GO in the  $\gamma$ -Fe<sub>2</sub>O<sub>3</sub>/GO composite. Fig. 1 b shows two typical peaks at 1336 cm<sup>-1</sup> (the D band represents disordered carbon) and at 1599 cm<sup>-1</sup> (the G band represents graphitic carbon). The intensity ratio of these two bands ( $I_D/I_G$ ) can be used to define the degree of structural defects and disorder in carbon materials (Mady et al., 2017). This ratio in the  $\gamma$ -Fe<sub>2</sub>O<sub>3</sub>/GO composite ( $I_D/I_G = 1.5$ ) was larger than that of GO where  $I_D/I_G = 1.09$  (Li et al., 2015), which indicates that an increase in disorder for the  $\gamma$ -Fe<sub>2</sub>O<sub>3</sub>/GO composite and also confirms that the GO has become partially reduced due to the presence of iron. To further

substantiate the formation of the  $\gamma$ -Fe<sub>2</sub>O<sub>3</sub>/GO composite, the low wave number region (400 cm<sup>-1</sup> to 1000 cm<sup>-1</sup>) was fine scanned; in the inset to Fig. 1b, it can be seen that the two broad bands at 495 and 700 cm<sup>-1</sup> belong to  $\gamma$ -Fe<sub>2</sub>O<sub>3</sub>. Moreover, these two bands were not present in any other spectra of iron oxide and the oxyhydroxide (Faria et al., 1997).

The thermal stability and thermal decomposition behavior of the synthetic composite were studied using the TGA technique. Fig. 1c shows three steps associated with weight loss as a function of temperature below 150 °C, 200–296 °C and 330–490 °C in the  $\gamma$ -Fe<sub>2</sub>O<sub>3</sub>/GO composite in an air atmosphere (Hu et al., 2015). The

weight loss below 150 °C was attributed to dehydration of free water. The second weight loss around 200 °C was presumed to be due to the decomposition of oxygen-containing groups on the surfaces of the GO (Wen et al., 2017). The third step from 330 °C to 490 °C was associated with the removal of the carbon skeleton due to the burning of the GO. Above 500 °C, the weight loss rate (derivative weight) was very small, indicating that the carbon skeleton was almost completely burnt out. At temperatures between 730 °C and 800 °C, the weight percent was constant at a value of 84% which can be considered as the Fe<sub>2</sub>O<sub>3</sub> content. Therefore, the mass percentage of  $\gamma$ -Fe<sub>2</sub>O<sub>3</sub> in the  $\gamma$ -Fe<sub>2</sub>O<sub>3</sub>/GO composite was estimated to be 84% from this self-assembly method.

The surface chemical compositions and electronic state of the  $\gamma$ -Fe<sub>2</sub>O<sub>3</sub>/GO composite were analyzed by XPS. The survey spectra (Fig. 2a) show the presence of the Fe 2p, O 1s and C 1s energy regions. The high-resolution Fe 2p spectrum in Fig. 2b reveals the two peaks at 710.5 eV and 724.1 eV of the binding energy of Fe 2p that correspond to Fe 2p<sub>3/2</sub> and Fe 2p<sub>1/2</sub>, respectively. There is almost no change in Fe 2p spectrum compared with pure Fe<sub>2</sub>O<sub>3</sub> nanoparticles (shown in Fig. S4a). The O 1s spectrum (Fig. 2c) can be deconvoluted into three different peaks at 529.3 eV, 530.7 eV and 532.1 eV. The peaks at 529.3 eV can be assigned to oxygen binding with Fe (Fe–O) (Qian et al., 2017a). The peak with binding energy of 530.7 eV can be assigned to the lattice hydroxyl with Fe (denoted as Fe–OH). Finally, the peak at 532.1 eV is deduced to be oxygen containing groups bonded with C atoms in GO (C–OH/C–O–C) (Liu et al., 2017a). However, for the Fe<sub>2</sub>O<sub>3</sub> nanoparticles (shown in Fig. S4b),

the area ratio of the Fe–O bonds increased, while the peak at 532.1 eV assigned to the C–OH/C–O–C greatly decreased because of the absence of the GO. Fig. 2d shows the C 1s spectrum that can be deconvoluted into four different peaks, indicating the C–C/C=C bonds (284.1 eV), the C–O bonds (epoxy and hydroxyl) at 286.2 eV, the C=O at O–C–O bonds (287.1 eV), and the O–C=O (carboxylate) bonds at 288.4 eV (Moussa et al., 2016).

The surface and cross-section morphology of the  $\gamma$ -Fe<sub>2</sub>O<sub>3</sub>/GO composite are shown in Fig. 3a and b, respectively. The  $\gamma$ -Fe<sub>2</sub>O<sub>3</sub>/GO composite has a wrinkled surface due to the rippled shape of the GO sheets, as shown in Fig. 3a. The thickness of the composite is about 1.2  $\mu$ m (Fig. 3b). The digital photo inset in Fig. 3b reveals its flake-like macroscopic morphology. This figure also suggests that the GO with iron oxides is assembled into a lamellar structure on the iron plates. Moreover, the thickness and the area of the  $\gamma$ -Fe<sub>2</sub>O<sub>3</sub>/GO composite could be controlled by volume of GO solution and its concentration. The presence of dense, sphere-like  $\gamma$ -Fe<sub>2</sub>O<sub>3</sub> nanoparticles anchored on the surface of the GO is apparent in the TEM images (shown in Fig. 3c). The  $\gamma$ -Fe<sub>2</sub>O<sub>3</sub> is well dispersed on the surface of the GO sheets, which can act to hinder aggregation and provide channels to promote mass transport (Zheng et al., 2015). The structure of GO sheets distributed with  $\gamma$ -Fe<sub>2</sub>O<sub>3</sub> nanoparticles could produce a synergistic effect by providing efficient charge/mass transfer between  $\gamma$ -Fe<sub>2</sub>O<sub>3</sub> nanoparticles and GO sheets, and thereby accelerating the Fenton-like processes and photocatalysis.

The Brunauer-Emmett-Teller (BET) specific surface area ( $S_{BET}$ ) of the  $\gamma$ -Fe<sub>2</sub>O<sub>3</sub>/GO composite was calculated to be 88.01 m<sup>2</sup>/g (shown

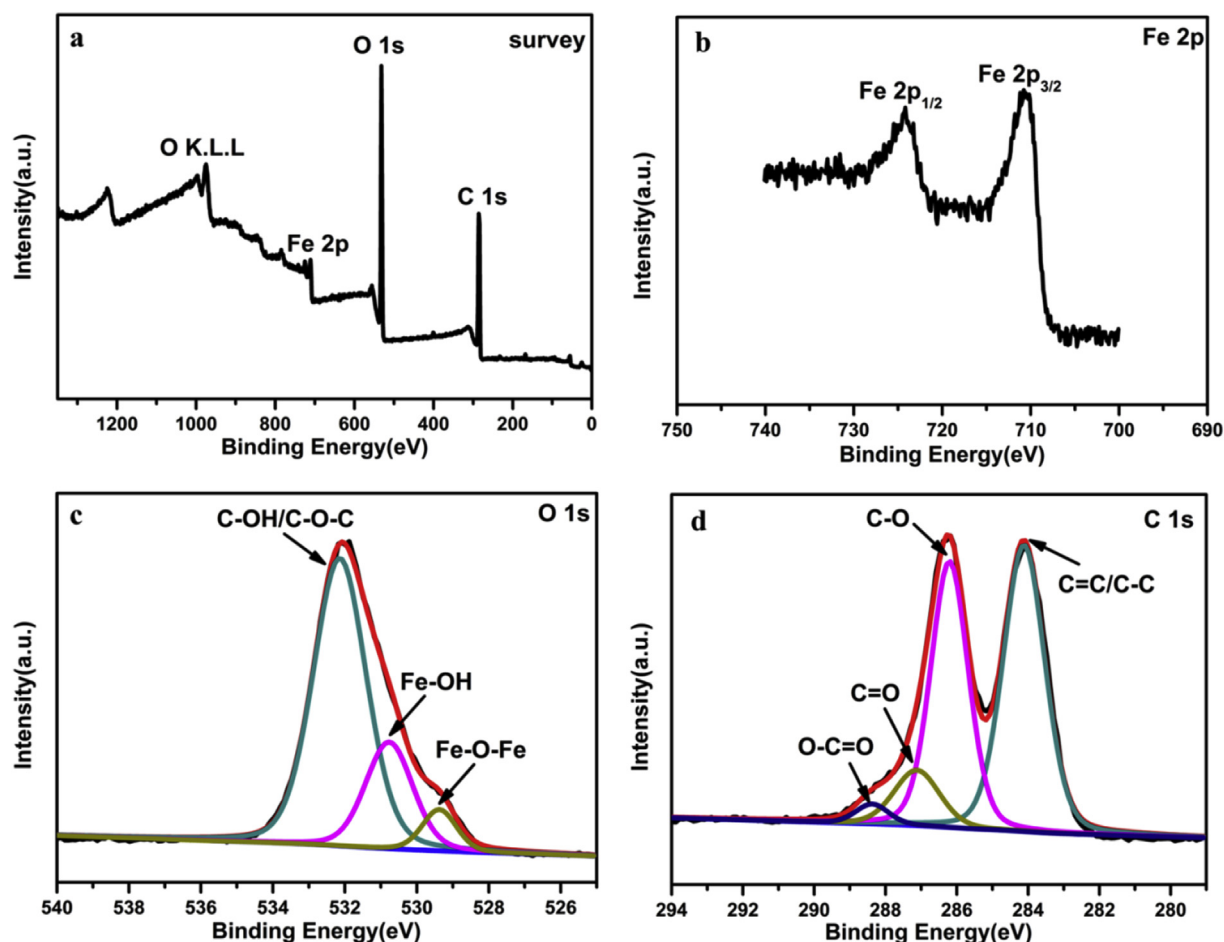


Fig. 2. XPS spectra of the  $\gamma$ -Fe<sub>2</sub>O<sub>3</sub>/GO composite: (a) survey scan, (b), (c) and (d) are high-resolution spectra of the Fe 2p, O 1s and C 1s, respectively.

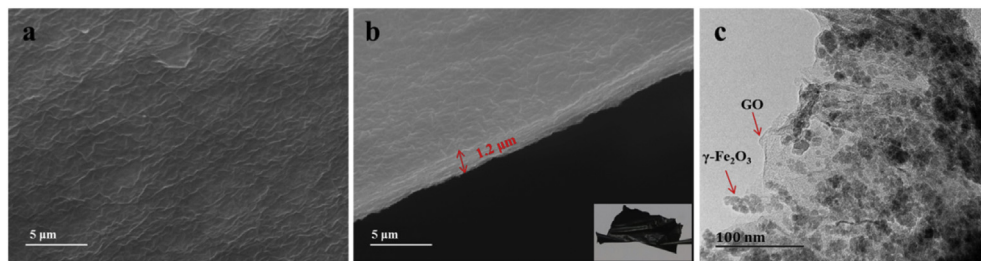


Fig. 3. SEM images of (a) the surface and (b) the cross-section of the  $\gamma$ -Fe<sub>2</sub>O<sub>3</sub>/GO composite; (c) TEM image of the  $\gamma$ -Fe<sub>2</sub>O<sub>3</sub>/GO composite.

in Fig. S5a) and the pore size distribution shows a sharp maximum at approximately 3.8 nm due to the existence of the mesoporous structure in the composite (shown in Fig. S5b). These mesoporous structures might provide more absorption or reaction sites to increase catalytic activity in the degradation process (Mady et al., 2017).

The prepared lamellar structure of  $\gamma$ -Fe<sub>2</sub>O<sub>3</sub>/GO composite catalyst was directly put into MB solution, which can easily be retrieved by a magnet. It can be seen in Fig. S6, the saturation magnetization (*M<sub>s</sub>*) of the  $\gamma$ -Fe<sub>2</sub>O<sub>3</sub>/GO composite has a value of 40.9 emu·g<sup>-1</sup>, which is lower than that of the  $\gamma$ -Fe<sub>2</sub>O<sub>3</sub> composite (52.6 emu·g<sup>-1</sup>), mainly due to the existence of the GO in the  $\gamma$ -Fe<sub>2</sub>O<sub>3</sub>/GO composite (Yang et al., 2015b). However, the *M<sub>s</sub>* of the  $\gamma$ -Fe<sub>2</sub>O<sub>3</sub>/GO composite is still large enough for the composite to be separated through an external magnetic field as shown in the inset in Fig. S6.

### 3.2. Catalytic activity measurements

The catalytic activity of the  $\gamma$ -Fe<sub>2</sub>O<sub>3</sub>/GO composite was studied for its effect on the degradation of the MB assisted by UV light. Fig. S7 shows two typical main peaks (614 nm and 664 nm) of MB spectra. The two peaks decreased with increasing time, and the solution gradually turned colorless within 80 min (shown in the inset of Fig. S7).

Fig. 4a shows the degree of decolorization of the MB under different conditions. The results in Fig. 4a clearly demonstrate the effects of the interaction among the decolorizing elements. It can be seen that the decolorization degree of the MB was very low for the use of UV photolysis alone (11% after 120 min). With the combination of H<sub>2</sub>O<sub>2</sub> and UV irradiation, the decolorization degree of the MB increased to 75%, which could be attributed to the •OH generated by H<sub>2</sub>O<sub>2</sub> under UV irradiation promoting the decomposition of chromophores in the MB molecules (Liu et al., 2017a). The decolorization degree of the MB slightly decreased to 63% when the GO was added into H<sub>2</sub>O<sub>2</sub>+UV system, which might be due to desorption of the MB on the surface of GO and large consumption of the H<sub>2</sub>O<sub>2</sub> in the later stage reaction. It was worth noting that the efficiency of decolorization could be significantly improved to 99% after 80 min when the  $\gamma$ -Fe<sub>2</sub>O<sub>3</sub>/GO composite was added to the H<sub>2</sub>O<sub>2</sub>+UV system, whereas the  $\gamma$ -Fe<sub>2</sub>O<sub>3</sub>/GO + H<sub>2</sub>O<sub>2</sub> + dark system that represented the Fenton-like process showed the decolorization degree of MB was only 25% after 120 min. The significant improvement of MB decolorization rate under UV irradiation is attributed to the photo-promoted decomposition of H<sub>2</sub>O<sub>2</sub> on the surface of  $\gamma$ -Fe<sub>2</sub>O<sub>3</sub>/GO composite to generate more reactive species •OH in the photo-Fenton system (Liu et al., 2017a). In addition, the  $\gamma$ -Fe<sub>2</sub>O<sub>3</sub>/GO + UV system without H<sub>2</sub>O<sub>2</sub> showed a 55% degree of MB decolorization after 120 min, and the low rate of MB decolorization indicated that only photocatalysis process could not efficiently achieve the complete MB decolorization, proving the importance of the synergy between photocatalysis and Fenton reactions. Furthermore, the decolorization degree of MB in  $\gamma$ -

Fe<sub>2</sub>O<sub>3</sub> + H<sub>2</sub>O<sub>2</sub> + UV system reached 84% after 120 min, and the only  $\gamma$ -Fe<sub>2</sub>O<sub>3</sub> nanoparticles without GO supports also owns a low rate of the MB degradation, implying that the ability of the hinder agglomeration and facilitated electrons transferring of the GO supports exert important effects on catalysis process.

The stability at different acidic conditions and reusability of the  $\gamma$ -Fe<sub>2</sub>O<sub>3</sub>/GO heterogeneous catalyst in the  $\gamma$ -Fe<sub>2</sub>O<sub>3</sub>/GO + H<sub>2</sub>O<sub>2</sub>+UV system are important factors for its practical application. The recyclability properties (Fig. 4b) were tested, and the catalytic activity of the  $\gamma$ -Fe<sub>2</sub>O<sub>3</sub>/GO composite examined at different initial pH from 2.0 to 10.2 (Fig. 4c). The MB decolorization ratio remained at near 99% after eight successive cycles, indicating its excellent stability and photo-Fenton activity. More importantly, the leaching of iron ions from the catalysts could not be detected or was at a rate lower than the ion detection limit of ICP-OES in the repeated cycles during experiment. This may result from the formation of Fe–O–H bonds which could enhance the chemical interaction between  $\gamma$ -Fe<sub>2</sub>O<sub>3</sub> and GO to suppress the iron ion leaching (Qian et al., 2017a). Thus, it can be inferred that the catalyst possesses excellent long term durability due to the strong interaction between  $\gamma$ -Fe<sub>2</sub>O<sub>3</sub> and GO, and can be repeatedly used with little loss of catalytic activities. The results in Fig. 4c show that the catalytic activity of the  $\gamma$ -Fe<sub>2</sub>O<sub>3</sub>/GO catalyst remained almost the same in the pH range from 4.2 to 10.2 with a high degree of decolorization of 99% within 100 min reaction. The good catalytic activity of the  $\gamma$ -Fe<sub>2</sub>O<sub>3</sub>/GO at a wide pH conditions might be attributed to the electronegative surface of the GO which tends to adsorb cationic MB molecules by  $\pi$ - $\pi$  stacking and electrostatic interactions (Liu et al., 2017a). Moreover, the interaction has a great influence on the affinity of the contaminant to the active sites (Liu et al., 2017b). In this system, the GO carries many negatively charged functional group at high pH, tending to enhance adsorption of the cationic MB molecules (Liu et al., 2012), which could facilitate the catalytic reaction. However, the decolorization rate was 93% after 100 min when the initial pH was 2.0. The slightly decreased decolorization rate may be ascribed to the strong acidity of the solution which restrains the adsorption of MB onto the surface of GO (Tang et al., 2005). Also, the formation of complex species [Fe(H<sub>2</sub>O)<sub>6</sub>]<sup>2+</sup> and stable oxonium ion [H<sub>3</sub>O<sub>2</sub>]<sup>+</sup> under conditions of high H<sup>+</sup> concentration can reduce the production of •OH. Indeed, Yang et al. (Yang et al., 2015a) reported that MB decolorization using the Fe/Fe<sub>3</sub>O<sub>4</sub>/GO composite was about 83% when the pH was 2. It can therefore be concluded that the  $\gamma$ -Fe<sub>2</sub>O<sub>3</sub>/GO catalyst displays great catalytic activity over a wide range of pH, and thus could be used in a broad spectrum of environmental conditions.

Apart from decolorization, the extent of MB mineralization is also important for industrial applications. The mineralization process was evaluated by TOC test. As shown in Fig. 4d, the TOC removal efficiency was 45% after 100min, while the 55% TOC left in the solution due to the generation of intermediates such as carboxyl acids (Liu et al., 2017a). In addition, the products concentration (SO<sub>4</sub><sup>2-</sup>) of the mineralization process associated with

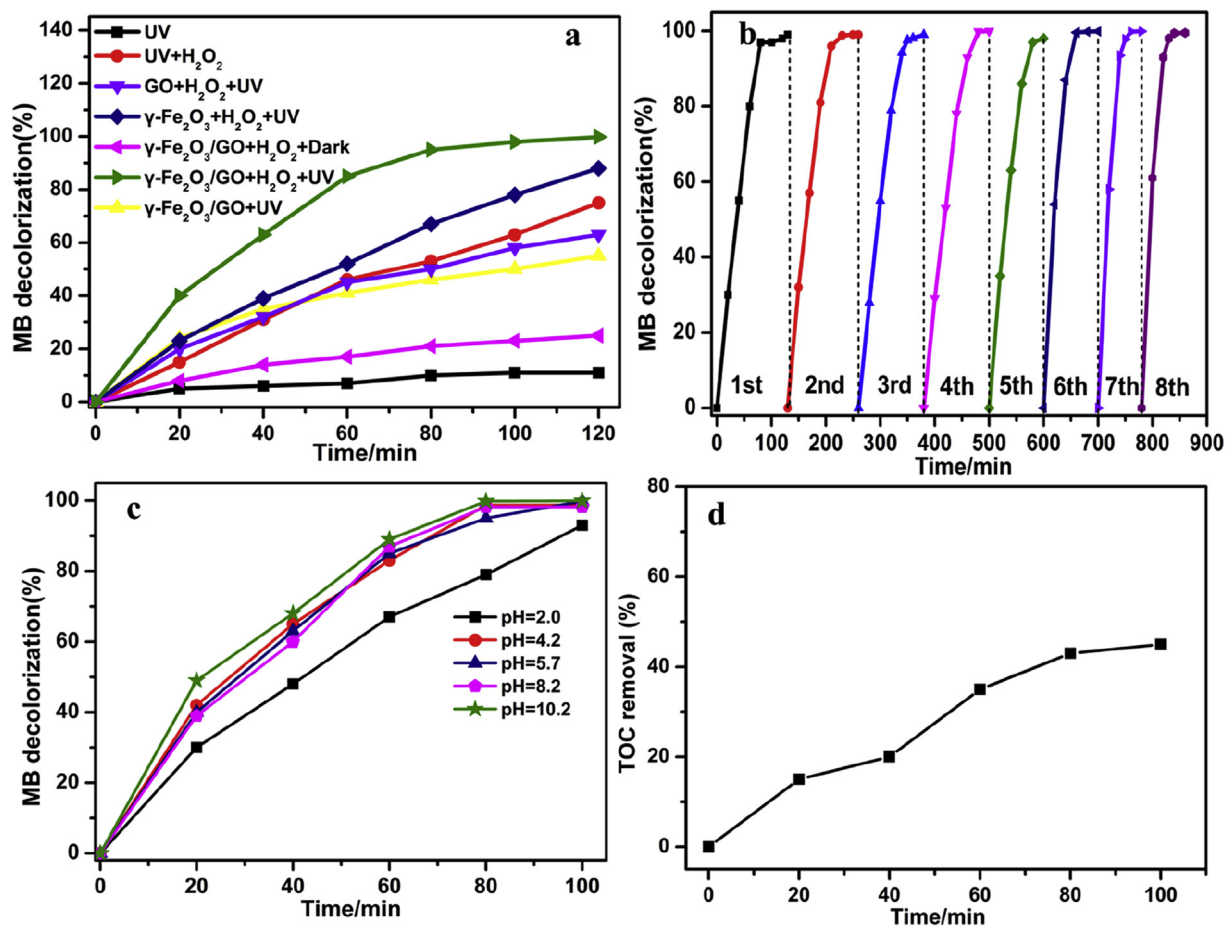


Fig. 4. (a) The decolorization of the MB under different conditions, (b) Repeated decolorization of MB solution of  $\gamma\text{-Fe}_2\text{O}_3/\text{GO}$  composite, (c) decolorization of the MB at different initial pHs. (d) TOC removal efficiency of the  $\gamma\text{-Fe}_2\text{O}_3/\text{GO}$  composite.

conversion of organic S-containing in MB solution was determined by ion chromatography. The concentration of  $\text{SO}_4^{2-}$  became  $11.3 \text{ mg L}^{-1}$  ( $0.5 \text{ mg L}^{-1} \text{ SO}_4^{2-}$  from  $\text{H}_2\text{O}_2$ ) after 100 min, while the theoretical value of the MB solution is  $12.8 \text{ mg L}^{-1}$ . A high mineralization rate of solution was achieved, indicating the high catalytic activity of the  $\gamma\text{-Fe}_2\text{O}_3/\text{GO}$  composite.

### 3.3. Catalytic mechanisms

Many studies have confirmed that the  $\bullet\text{OH}$  and  $\bullet\text{O}_2^-$  are the principal radicals detected using quenching experiments or electron spin resonance spectroscopy in photo-assisted iron oxide Fenton systems (Qian et al., 2017b; Wang et al., 2018a; Zhang et al., 2018a). In this study, methanol (MeOH), p-benzoquinone (BQ) and triethanolamine (TEOA) were added to this catalytic system as obligate  $\bullet\text{OH}$ ,  $\bullet\text{O}_2^-$  and holes scavengers, respectively. In the following, we first explore the photocatalytic mechanism of  $\gamma\text{-Fe}_2\text{O}_3/\text{GO}$  composite as a representative case. Fig. 5a shows the quenching effect on MB decolorization in the  $\gamma\text{-Fe}_2\text{O}_3/\text{GO}$  heterogeneous composite catalyst. It can be seen that MB decolorization is significantly suppressed in the presence of MeOH and TEOA, while adding BQ had a slight influence on MB decolorization, implying that the species of  $\bullet\text{OH}$  produced mainly through Fenton-like process and holes through photocatalysis are the dominant radicals during the decolorization process. The Photoluminescence spectra (PL) technique was utilized to confirm the generation of  $\bullet\text{OH}$  by using terephthalic acid (TA) as a probe molecule. Fig. 5b

shows the PL of  $\gamma\text{-Fe}_2\text{O}_3/\text{GO} + \text{H}_2\text{O}_2 + \text{UV}$  systems in the presence of TA. A gradual increase in PL intensity with increasing time is observed, indicating that the amount of  $\bullet\text{OH}$  generated by the system increased with time. Therefore, the high decolorizing efficiency of the  $\gamma\text{-Fe}_2\text{O}_3/\text{GO} + \text{H}_2\text{O}_2 + \text{UV}$  system comes from the synergistic effects of Fenton-like process and photocatalysis, while the other systems with only one process, either Fenton-like process or photolysis, have relatively low decolorization rates. Moreover, the  $\gamma\text{-Fe}_2\text{O}_3/\text{GO}$  composite owns a smaller Nyquist arc radius than the  $\gamma\text{-Fe}_2\text{O}_3$  nanoparticles, indicative of the improvement in charge transfer efficiency and the suppression of charge recombination of the  $\gamma\text{-Fe}_2\text{O}_3/\text{GO}$  composite (as shown in Fig. 5c). Therefore, a higher catalytic activity of  $\gamma\text{-Fe}_2\text{O}_3/\text{GO}$  composite could be achieved.

Based on the above mentioned experimental details and specific analysis, a schematic illustration of positive synergistic effect between the photocatalysis and Fenton reactions is given in Fig. 6. Firstly, the MB molecule can be adsorbed on the surface of the GO sheets through electrostatic interactions and  $\pi\text{-}\pi$  stacking (Liu et al., 2017a). At the same time, there are three main processes that probably can decompose the MB molecule. The first process is the Fenton-like reaction and the recycling of  $\text{Fe(III)}/\text{Fe(II)}$  is very important to this reaction. During this process, the  $\text{Fe(III)}$  reacted with  $\text{H}_2\text{O}_2$  to produce  $\bullet\text{OOH}$  and  $\text{Fe(II)}$  (Eq. (1)), and the  $\bullet\text{OH}$  was formed through a reaction of the generated  $\text{Fe(II)}$  with  $\text{H}_2\text{O}_2$  (Eq. (2)) (Zhang et al., 2018c). However, the reaction rate was relatively slow due to the low conversion of  $\text{Fe(III)}$  to  $\text{Fe(II)}$  by reacting with  $\text{H}_2\text{O}_2$ , which inhibited the generation of  $\bullet\text{OH}$  and then reduced the

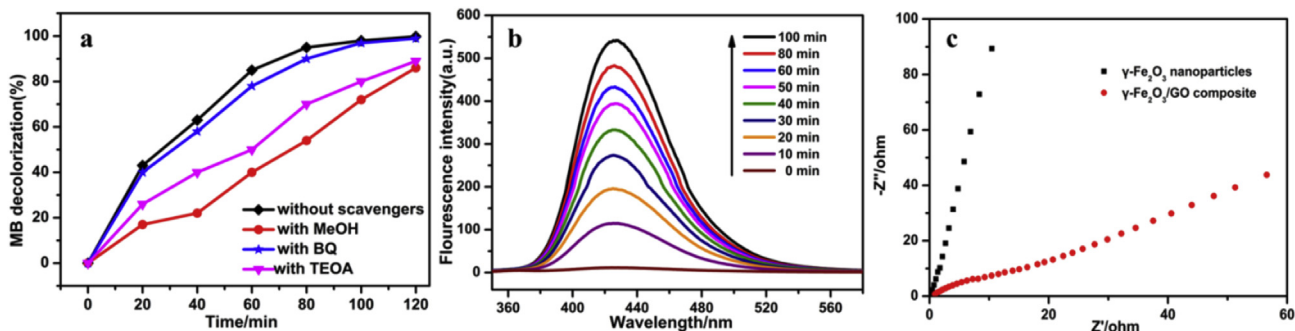


Fig. 5. MB decolorization in presence of radical scavengers, PL spectra changed with UV light irradiation time on  $\gamma\text{-Fe}_2\text{O}_3/\text{GO}$  composite, EIS Nyquist impedance plots of  $\gamma\text{-Fe}_2\text{O}_3$  nanoparticles and  $\gamma\text{-Fe}_2\text{O}_3/\text{GO}$  composite.

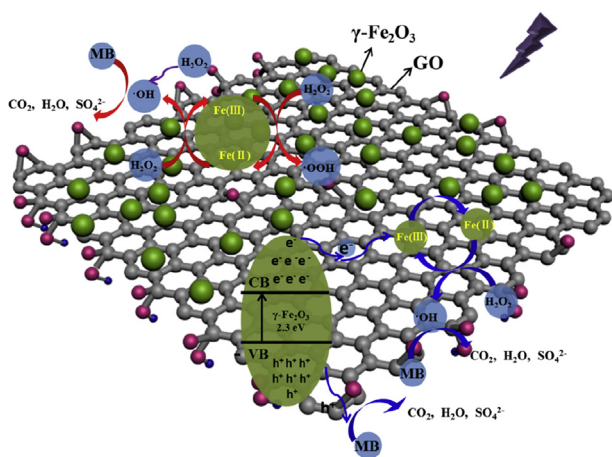
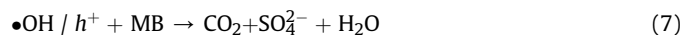
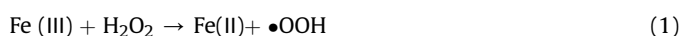


Fig. 6. Schematic illustration of the proposed mechanism for MB degradation of  $\gamma\text{-Fe}_2\text{O}_3/\text{GO}$  catalyst under UV irradiation.

MB decolorization rate (as confirmed by pink curve in Fig. 4a). The second process is the photocatalytic process. The  $\gamma\text{-Fe}_2\text{O}_3$  nanoparticles with a band gap of 2.30 eV could be activated to produce electrons and holes ( $e^-$  and  $h^+$ ) pairs in the conduction bands and valence bands, respectively (Eq. (3)) (Beydoun et al., 2000). These electrons were transferred to GO surface and reacted with  $\text{O}_2$  to form  $\bullet\text{O}_2^-$ , while the holes can degrade MB through a direct holes oxidation mechanism (Wang et al., 2018b). In this process, on one hand the quenching experiments proved that the  $\bullet\text{O}_2^-$  was not the main active species (as shown in Fig. 5a blue curve); on the other hand, only photocatalytic process owned a low rate of MB decolorization (as shown in Fig. 4a yellow curve). Therefore, a mechanism of synergy between photocatalysis and Fenton-like reaction is proposed. The electrons photo-generated from the  $\gamma\text{-Fe}_2\text{O}_3$  nanoparticles were transferred to GO surface which could hinder the recombination of electrons and holes pairs. Then the Fe(III) captured the electrons to form Fe(II) that can further react with  $\text{H}_2\text{O}_2$  to produce  $\bullet\text{OH}$  and Fe(III) (Eqs. (2) and (4)), the cycle reaction of Fe(III)/Fe(II) was therefore accelerated. In addition, the electrons captured by  $\text{H}_2\text{O}_2$  to form  $\bullet\text{OH}$  (Eq. (5)) and  $\text{H}_2\text{O}_2$  can directly produce  $\bullet\text{OH}$  under UV irradiation (Eq. (6)). Hydroxyl radicals had a strong oxidation potential and can thus oxidize MB into  $\text{CO}_2$ ,  $\text{SO}_4^{2-}$  and other inorganic substances (Wu et al., 2018). Moreover, the photo-generated holes can directly oxidize MB (Eq. (7)). The mechanisms can be explained through the following reactions:



The charge separation and suppression of carrier recombination due to the synergistic interaction between  $\gamma\text{-Fe}_2\text{O}_3$  and GO are realized, which can accelerate the Fenton-like process and photocatalysis. Therefore, the  $\gamma\text{-Fe}_2\text{O}_3/\text{GO}$  catalyst prepared by our self-assembly method appears to markedly enhance the degradation of the MB under UV irradiation though synergistic interactions between GO supports and the  $\gamma\text{-Fe}_2\text{O}_3$  nanoparticles.

#### 4. Conclusions

A novel and facile self-assembly method is demonstrated to successfully synthesize a  $\gamma\text{-Fe}_2\text{O}_3/\text{GO}$  heterogeneous catalyst on iron plates. The  $\gamma\text{-Fe}_2\text{O}_3/\text{GO}$  composite exhibited excellent photo-Fenton catalytic activity. The MB degradation was completed within 80 min with the  $\gamma\text{-Fe}_2\text{O}_3/\text{GO} + \text{H}_2\text{O}_2 + \text{UV}$  system. The high decolorizing efficiency can be attributed to the synergistic effects of Fenton-like process and photocatalysis. It is found that the charge separation at the  $\gamma\text{-Fe}_2\text{O}_3$  and GO interface can suppress the carrier recombination, such that the  $\bullet\text{OH}$  formed through interaction between electron and  $\text{H}_2\text{O}_2$  together with photo-generated holes both can oxidize MB. In addition, the composite catalyst was re-used for 8 cycles with little loss of catalytic activities, it can be effectively used over a wide pH range (2.0–10.2), and can be readily separated from the solution using a magnet; these beneficial factors demonstrate the potential of the catalyst for practical applications in dye water treatment. The overall preparation, separation and re-use of the  $\gamma\text{-Fe}_2\text{O}_3/\text{GO}$  catalyst would likely reduce operational costs and increase degradation productivity, which presents a new possibility for the clean-up a major environmental issues, that of wastewater treatment to remove colored dyes.

#### Acknowledgments

The authors would like to thank the financial support and the experimental facilities of the International Research Centre for Advanced Structural and Bio-Materials, Beihang University, Beijing,

China. This project was supported by the National Natural Science Foundation of China (91544227, 21407152, 21590811). The authors declare that they have no conflict of interest.

## Appendix A. Supplementary data

Supplementary data to this article can be found online at <https://doi.org/10.1016/j.envpol.2019.01.018>.

## References

- Beydoun, D., Amal, R., Low, G.K.C., Mcevoy, S., 2000. Novel Photocatalyst: titania-coated magnetite. Activity and photodissolution. *J. Phys. Chem. B* 104, 4387–4396.
- Cao, X., Qi, D., Yin, S., Bu, J., Li, F., Goh, C.F., Zhang, S., Chen, X., 2013. Ambient fabrication of large-area graphene films via a synchronous reduction and assembly strategy. *Adv. Mater.* 25, 2957–2962.
- Chen, X., Chen, B., 2018. Facile fabrication of crumpled graphene oxide nanosheets and its Platinum nano-hybrids for high efficient catalytic activity. *Environ. Pollut.* 243, 1810–1817.
- Cheng, M., Ma, W., Li, J., Yingping Huang, A., Zhao, J., Wen, Y.X., Xu, Y., 2004. Visible-light-assisted degradation of dye pollutants over Fe(III)-Loaded resin in the presence of H<sub>2</sub>O<sub>2</sub> at neutral pH values. *Environ. Sci. Technol.* 38, 1569–1575.
- Dong, Y., Wang, T., Wan, X., He, D., 2015. Washing and dyeing wastewater treatment by combined nano flocculation and photocatalysis processes. *J. Geosci. Environ. Protect.* 3, 66–71.
- Dong, C., Lu, J., Qiu, B., Shen, B., Xing, M., Zhang, J., 2018. Developing stretchable and graphene-oxide-based hydrogel for the removal of organic pollutants and metal ions. *Appl. Catal. B Environ.* 222, 146–156.
- Faria, D.L.A.D., Silva, S.V., Oliveira, M.T.D., 1997. Raman microspectroscopy of some iron oxides and oxyhydroxides. *J. Raman Spectrosc.* 28, 873–878.
- Guo, S., Zhang, G., Guo, Y., Jimmy, C.Y., 2013. Graphene oxide–Fe<sub>2</sub>O<sub>3</sub> hybrid material as highly efficient heterogeneous catalyst for degradation of organic contaminants. *Carbon* 60, 437–444.
- Guo, S., Zhang, G., Wang, J., 2014. Photo-Fenton degradation of rhodamine B using Fe<sub>2</sub>O<sub>3</sub>-Kaolin as heterogeneous catalyst: characterization, process optimization and mechanism. *J. Colloid Interface Sci.* 433, 1–8.
- Han, S., Hu, L., Liang, Z., Wageh, S., Al-Ghamdi, A.A., Chen, Y., Fang, X., 2014. One-step hydrothermal synthesis of 2D hexagonal nanoplates of  $\alpha$ -Fe<sub>2</sub>O<sub>3</sub>/graphene composites with enhanced photocatalytic activity. *Adv. Funct. Mater.* 24, 5719–5727.
- Hu, Z.T., Lua, S.K., Lim, T.T., 2015. Cuboid-like Bi<sub>2</sub>Fe<sub>4</sub>O<sub>9</sub>/Ag with graphene-wrapping tribrid composite with superior capability for environmental decontamination: nanoscaled material design and visible-light-driven multifunctional catalyst. *ACS Sustain. Chem. Eng.* 3, 2726–2736.
- Jin, Q., Zhang, S., Wen, T., Wang, J., Gu, P., Zhao, G., Wang, X., Chen, Z., Hayat, T., Wang, X., 2018. Simultaneous adsorption and oxidative degradation of Bisphenol A by zero-valent iron/iron carbide nanoparticles encapsulated in N-doped carbon matrix. *Environ. Pollut.* 243, 218–227.
- Li, P.F., Xu, Y., Cheng, X.H., 2013. Chemisorption of thermal reduced graphene oxide nano-layer film on TNTZ surface and its tribological behavior. *Surf. Coating Technol.* 232, 331–339.
- Li, Y., Qu, J., Gao, F., Lv, S., Lin, S., He, C., Sun, J., 2015. In situ fabrication of Mn<sub>3</sub>O<sub>4</sub> decorated graphene oxide as a synergistic catalyst for degradation of methylene blue. *Appl. Catal. B Environ.* 162, 268–274.
- Li, S., Zhang, G., Zhang, W., Zheng, H., Zhu, W., Sun, N., Zheng, Y., Wang, P., 2017. Microwave enhanced Fenton-like process for degradation of perfluorooctanoic acid (PFOA) using Pb-BiFeO<sub>3</sub>/rGO as heterogeneous catalyst. *Chem. Eng. J.* 326, 756–764.
- Liu, F., Chung, S., Oh, G., Seo, T.S., 2012. Three-dimensional graphene oxide nanostructure for fast and efficient water-soluble dye removal. *ACS Appl. Mater. Interfaces* 4, 922–927.
- Liu, X., Zhang, Q., Yu, B., Wu, R., Mai, J., Wang, R., Chen, L., Yang, S.T., 2016. Preparation of Fe<sub>3</sub>O<sub>4</sub>/TiO<sub>2</sub>/C nanocomposites and their application in Fenton-like catalysis for dye decoloration. *Catalysts* 6, 146.
- Liu, Y., Jin, W., Zhao, Y., Zhang, G., Zhang, W., 2017a. Enhanced catalytic degradation of methylene blue by  $\alpha$ -Fe<sub>2</sub>O<sub>3</sub>/graphene oxide via heterogeneous photo-Fenton reactions. *Appl. Catal. B Environ.* 206, 642–652.
- Liu, Y., Liu, X., Zhao, Y., Dionysiou, D.D., 2017b. Aligned  $\alpha$ -FeOOH nanorods anchored on a graphene oxide-carbon nanotubes aerogel can serve as an effective Fenton-like oxidation catalyst. *Appl. Catal. B Environ.* 213, 74–86.
- Liu, X., Xu, X., Sun, J., Duan, S., Sun, Y., Hayat, T., Li, J., 2018. Interaction between Al<sub>2</sub>O<sub>3</sub> and different sizes of GO in aqueous environment. *Environ. Pollut.* 243, 1802–1809.
- Macedo, A.L., Fabris, J.D., Pires, M.J.M., Oliveira, W.L., Ardisson, J.D., Augusti, R., Aragón, F.H., Santos, R.S., Oliveira, L.C.A., Pereira, M.C., 2016. A mesoporous SiO<sub>2</sub>/ $\gamma$ -Fe<sub>2</sub>O<sub>3</sub>/KI heterogeneous magnetic catalyst for the green synthesis of biodiesel. *J. Braz. Chem. Soc.* 27, 2290–2299.
- Mady, A.H., Baynosa, M.L., Tuma, D., Shim, J.J., 2017. Facile microwave-assisted green synthesis of Ag-ZnFe<sub>2</sub>O<sub>4</sub>@rGO nanocomposites for efficient removal of organic dyes under UV- and visible-light irradiation. *Appl. Catal. B Environ.* 203, 416–427.
- Maleki, H., 2016. Recent advances in aerogels for environmental remediation applications: a review. *Chem. Eng. J.* 300, 98–118.
- Moussa, H., Giro, E., Mozet, K., Alem, H., Medjahdi, G., Schneider, R., 2016. ZnO rods/reduced graphene oxide composites prepared via a solvothermal reaction for efficient sunlight-driven photocatalysis. *Appl. Catal. B Environ.* 185, 11–21.
- Munoz, M., De Pedro, Z.M., Casas, J.A., Rodriguez, J.J., 2015. Preparation of magnetite-based catalysts and their application in heterogeneous Fenton oxidation—a review. *Appl. Catal. B Environ.* 176, 249–265.
- Muthukrishnaraj, A., Vadivel, S., Kamalakannan, V.P., Balasubramanian, N., 2015.  $\alpha$ -Fe<sub>2</sub>O<sub>3</sub>/reduced graphene oxide nanorod as efficient photocatalyst for methylene blue degradation. *Mater. Res. Innovat.* 19, 258–264.
- Parra, S., Henao, L., Mielczarski, E., Mielczarski, J., Albers, P., Suvorova, E., Guindet, J., 2004. Synthesis, testing, and characterization of a novel Nafion membrane with superior performance in photoassisted immobilized Fenton catalysis. *Langmuir* 20, 5621–5629.
- Qian, X., Meng, R., Yao, Z., Yue, D., Yu, H., Jia, J., Zhao, Y., 2017a. Visible light assisted heterogeneous Fenton-like degradation of organic pollutant via  $\alpha$ -FeOOH/mesoporous carbon composites. *Environ. Sci. Technol.* 51, 3993–4000.
- Qian, X., Ren, M., Zhu, Y., Yue, D., Han, Y., Jia, J., Zhao, Y., 2017b. Visible light assisted heterogeneous Fenton-like degradation of organic pollutant via  $\alpha$ -FeOOH/mesoporous carbon composites. *Environ. Sci. Technol.* 51, 3993–4000.
- Qiu, B., Xing, M., Zhang, J., 2015. Stöber-like method to synthesize ultralight, porous, stretchable Fe<sub>2</sub>O<sub>3</sub>/graphene aerogels for excellent performance in photo-Fenton reaction and electrochemical capacitors. *J. Mater. Chem. A* 3, 12820–12827.
- Tang, J., Zou, Z., Ye, J., 2005. Kinetics of MB degradation and effect of pH on the photocatalytic activity of Mn<sub>2</sub>O<sub>4</sub> (M = Ca, Sr, Ba) under visible light irradiation. *Res. Chem. Intermed.* 31, 513–519.
- Techalerthanee, T., Chancharoenrith, S., Namkajorn, M., Kiattisevi, S., Chaicharoenwimolkul, L., Somsook, E., 2015. Facile synthesis of zinc–iron mixed oxide/carbon nanocomposites as nanocatalysts for the degradation of methylene blue. *Mater. Lett.* 145, 224–228.
- Triki, M., Contreras, S., Medina, F., 2014. Pd–Fe/TiO<sub>2</sub> catalysts for phenol degradation with in situ generated H<sub>2</sub>O<sub>2</sub>. *J. Sol. Gel Sci. Technol.* 71, 96–101.
- Wang, X., Liu, C., Li, X., Li, F., Zhou, S., 2008. Photodegradation of 2-mercaptobenzothiazole in the gamma-Fe(2)O(3)/oxalate suspension under UVA light irradiation. *J. Hazard Mater.* 153, 426–433.
- Wang, J., Liu, C., Qi, J., Li, J., Sun, X., Shen, J., Han, W., Wang, L., 2018a. Enhanced heterogeneous Fenton-like systems based on highly dispersed FeO-Fe<sub>2</sub>O<sub>3</sub> nanoparticles embedded ordered mesoporous carbon composite catalyst. *Environ. Pollut.* 243, 1068–1077.
- Wang, W., An, T., Li, G., Li, Y., Jimmy, C.Y., Wong, P.K., 2018b. Free-standing red phosphorus/silver sponge monolith as an efficient and easily recyclable macroscale photocatalyst for organic pollutant degradation under visible light irradiation. *J. Colloid Interface Sci.* 518, 130–139.
- Wen, T., Wang, J., Yu, S., Chen, Z., Hayat, T., Wang, X., 2017. Magnetic porous carbonaceous material produced from tea waste for efficient removal of as (V), Cr (VI), humic acid, and dyes. *ACS Sustain. Chem. Eng.* 5, 4371–4380.
- William Jr., S.H., Offeman, R.E., 1958. Preparation of graphitic oxide. *J. Am. Chem. Soc.* 80, 1339.
- Wu, X.Q., Shen, J.S., Zhao, F., Shao, Z.D., Zhong, L.B., Zheng, Y.M., 2018. Flexible electrospun MWCNTs/Ag<sub>3</sub>PO<sub>4</sub>/PAN ternary composite fiber membranes with enhanced photocatalytic activity and stability under visible-light irradiation. *J. Mater. Sci.* 53, 10147–10159.
- Yang, B., Tian, Z., Zhang, L., Guo, Y., Yan, S., 2015a. Enhanced heterogeneous Fenton degradation of Methylene Blue by nanoscale zero valent iron (nZVI) assembled on magnetic Fe<sub>3</sub>O<sub>4</sub>/reduced graphene oxide. *J. Water Proc. Eng.* 5, 101–111.
- Yang, X., Chen, W., Huang, J., Zhou, Y., Zhu, Y., Li, C., 2015b. Rapid degradation of methylene blue in a novel heterogeneous Fe<sub>3</sub>O<sub>4</sub>@rGO/TiO<sub>2</sub>-catalyzed photo-Fenton system. *Sci. Rep.* 5, 10632.
- Yu, L., Chen, J., Liang, Z., Xu, W., Chen, L., Ye, D., 2016. Degradation of phenol using Fe<sub>3</sub>O<sub>4</sub>-GO nanocomposite as a heterogeneous photo-Fenton catalyst. *Separ. Purif. Technol.* 171, 80–87.
- Zhang, X., Liu, D., Yang, L., Zhou, L., You, T., 2015. Self-assembled three-dimensional graphene-based materials for dye adsorption and catalysis. *J. Mater. Chem. A* 3, 10031–10037.
- Zhang, J., Yao, T., Guan, C., Zhang, N., Zhang, H., Zhang, X., Wu, J., 2017. One-pot preparation of ternary reduced graphene oxide nanosheets/Fe<sub>2</sub>O<sub>3</sub>/poly-pyrrole hydrogels as efficient Fenton catalysts. *J. Colloid Interface Sci.* 505, 130.
- Zhang, S., Gao, H., Huang, Y., Wang, X., Hayat, T., Li, J., Xu, X., Wang, X., 2018a. Ultrathin g-C<sub>3</sub>N<sub>4</sub> nanosheets coupled with amorphous Cu-doped FeOOH nanoclusters as 2D/0D heterogeneous catalysts for water remediation. *Environ. Sci.: Nano* 5, 1179–1190.
- Zhang, S., Gu, P., Ma, R., Luo, C., Wen, T., Zhao, G., Cheng, W., Wang, X., 2018b. Recent developments in fabrication and structure regulation of visible-light-driven g-C<sub>3</sub>N<sub>4</sub>-based photocatalysts towards water purification: a critical review. *Catal. Today*. <https://doi.org/10.1016/j.cattod.2018.09.013>.

- Zhang, Y., Chen, Z., Zhou, L., Wu, P., Zhao, Y., Lai, Y., Wang, F., 2018c. Heterogeneous Fenton degradation of bisphenol A using  $\text{Fe}_3\text{O}_4@ \beta\text{-CD/rGO}$  composite: synergistic effect, principle and way of degradation. *Environ. Pollut.* <https://doi.org/10.1016/j.envpol.2018.10.028>.
- Zheng, Q., Cai, Z., Ma, Z., Gong, S., 2015. Cellulose nanofibril/reduced graphene oxide/carbon nanotube hybrid aerogels for highly flexible and all-solid-state supercapacitors. *ACS Appl. Mater. Interfaces* 7, 3263–3271.
- Zhou, Q., Lin, Y., Zhang, K., Li, M., Tang, D., 2018. Reduced graphene oxide/ $\text{BiFeO}_3$  nanohybrids-based signal-on photoelectrochemical sensing system for prostate-specific antigen detection coupling with magnetic microfluidic device. *Biosens. Bioelectron.* 101, 146–152.